ACS OMEGA

http://pubs.acs.org/journal/acsodf

Article

Ignition Delay Time and Oxidation of a Kerosene Aviation Fuel and a Blended Jet50-Bio50 Fuel

Cheon Hyeon Cho, Hee Sun Han, Chae Hoon Sohn,* and Jeong Sik Han

Cite This: *ACS Omega* 2021, 6, 26646−26658

Read Online

ACCESS | Metrics & More | Article Recommendations

ABSTRACT: Ignition delay and oxidation of two jet aviation fuels, Jet A-1 and its blended fuel with a bio-jet fuel in half, are investigated by experiments and numerical simulations. From their major combustion properties, derived cetane number and molecular weight of the blended fuel, Jet50-Bio50, are higher than those of Jet A-1, and its H/C ratio and threshold sooting index are lower because more *n*-alkanes are contained in a bio-jet fuel and aromatic compounds are not. The surrogate fuels of the two jet fuels are constructed for numerical simulations of their ignition and oxidation. Early ignition of the blended fuel measured in a shock tube experiment is investigated by comparing the speciation profiles of several products from the two fuels, and their global reactivity is measured in a laminar flow reactor. Oxidation of the blended fuel is initiated at a lower temperature than Jet A-1, and reaction pathways of the two fuels are analyzed at two temperatures of 600 and 1100 K, respectively. At a low temperature of 600 K, reaction pathways of the major surrogate components for the two fuels are significantly different, while they are almost the same at high temperatures. The active radical of OH is produced more by the oxidation of Jet50-Bio50, and its oxidation is initiated at a lower temperature than Jet A-1, leading to earlier ignition. At low temperatures, the difference between initiation times of oxidation of the two fuels is much larger than at high temperatures. At both temperatures, production rates of the major reaction steps, where OH is produced, are higher in Jet50-Bio50 than in Jet A-1.

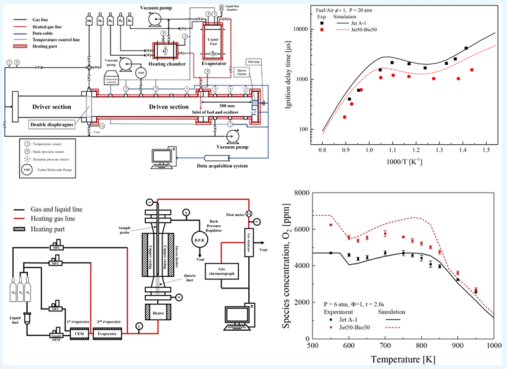

1. INTRODUCTION

Conventional jet aviation fuel is a mixture of hundreds of different hydrocarbons extracted from middle distillates of crude oil. A typical jet fuel is a kerosene which has a broad carbon-number distribution mainly from 8 to 16. Kerosene such as Jet A or Jet A-1 is composed of n-paraffins, branched iso-alkanes, cyclic alkanes, and aromatics.[1,2] It has been widely used for jet propulsion and consumed in a large amount in propulsion systems. However, it will be depleted in the end since it is one of the petroleum-based fossil fuels. Furthermore, its burning produces air pollutants such as soot, CO, CO_2, and NO_x, and thereby, conventional jet fuels are confronted with environmental issues of particulates and global warming. For these reasons and fuel flexibility, the aviation industry is pursuing alternative fuels such as renewable and environment-friendly fuels. A bio-jet fuel is one of the promising alternative fuels for jet propulsion due to less aromatic contents and carbon neutral properties.[3] However, its feasibility should be verified first before its application to a bio-jet to jet engines.

There can be found several previous works relevant to the production and utilization of bio-jet fuels. Yang et al.[1] evaluated the performance of bio-jet fuels based on low-temperature fluidity, thermal oxidation stability, combustion properties, fuel compatibility, and physicochemical properties including volatility and energy density. This work also reported that the aromatic content had a significant impact on the performance of bio-jet fuels. Wei et al.[2] reported bio-jet fuel conversion technology, economic evaluation, environmental impact, and development status. This work suggested that hydrogenated esters and the fatty acid process and Fischer−Tropsch synthesis[4] could become the most popular techniques for bio-jet fuel production in the near future and reported that bio-jet fuels from biomass feedstocks had significant potential for reducing CO_2 emissions. Goel and Boehman[5] studied the degradation of jet fuel using a flow reactor. *N*-dodecane was adopted as a surrogate fuel to simulate jet fuel and outlet bulk temperature, and the unreacted fuel fraction was predicted as the flow rate increased. Pelucchi et al.[6] conducted experiments using a jet-stirred reactor to develop a surrogate model for fast pyrolysis bio-oil (FPBO) extracted from lignocellulosic biomass. In particular, thermal decomposition and combustion chemistry of pyrrole (C_4H_5N), a candidate reference fuel for the FPBO surrogate model, were

Received: July 27, 2021
Accepted: September 24, 2021
Published: October 1, 2021

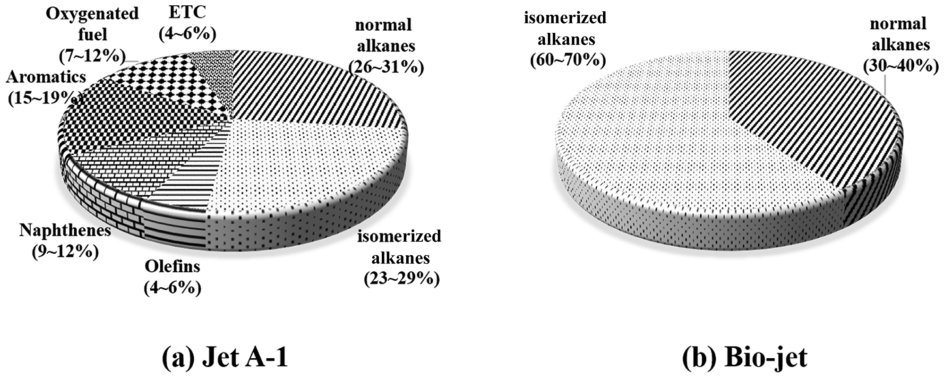

Figure 1. Molecular-class compositions of (a) Jet A-1 and (b) bio-jet identified by the relative signal area percentage analysis of GC−MS.

studied. Zeng et al.[7] studied the pyrolysis of the RP-3 jet fuel using a single-pulse shock tube (SPST) and found that ethylene was the most abundant product. In addition, it was confirmed that methane, ethane, and propene were present in a large amount, and acetylene increased significantly as the temperature increased. Wang et al.[8] performed a thermal decomposition study on the mixing of the direct coal liquefaction (DCL)-derived jet fuel and conventional RP-3 jet fuel using a SPST. This work showed that the formation of 1,3-butadiene is the main difference between RP-3 and its derived jet fuel.

Recently, Han et al.[9] reported that a mixture of Jet A-1 and a bio-jet fuel available in Korea could be a substitute for Jet A-1 and is adaptable to an existing jet engine in terms of ignition and emission. The mixture is called Jet50-Bio50, which is produced by blending Jet A-1 with a bio-jet fuel in the same ratio, that is, 50:50 in volume fraction. The adopted bio-jet fuel was developed using the biomass produced in Korea, and it was made by the Fischer−Tropsch process.[4] Moreover, it is mostly composed of normal and isomerized alkanes.

From the previous work,[9] it was found that Jet50-Bio50, the mixture of Jet A-1 and a bio-jet fuel, has the characteristics of earlier ignition and lower emission than Jet A-1, which is more desirable in application to aero-propulsion than a conventional jet fuel. Lower emission can be easily predicted by no aromatic contents contained in a bio-jet fuel. However, earlier ignition of the mixture was not clarified and information on the phenomenon was not provided sufficiently. In this regard, ignition and oxidation of the mixture, Jet50-Bio50, are studied here by experiments and numerical simulations to find its reaction characteristics distinct from the oxidation of a convention jet fuel, Jet A-1.

2. METHODOLOGIES

2.1. Fuel Properties and Surrogate Fuels. The fuel compositions of Jet A-1 and the bio-jet fuel are shown in Figure 1, respectively. As can be seen in the figure, there are discrepancies in compositions between the two fuels. The mixture of Jet A-1 and the bio-jet fuel, that is, Jet50-Bio50, has more alkanes than Jet A-1and no aromatics.

The carbon distributions of components of Jet A-1 and Jet50-Bio50 from C7 to C17 are shown in Figure 2. Both Jet A-1 and Jet50-Bio50 contain more isomerized alkanes than normal alkanes over the full range of carbon numbers. Normal alkanes start to react at a lower temperature than *iso*-alkanes, and they would play a critical role in the earlier oxidation of the fuel. Jet A-1 has more normal alkanes with carbon numbers from 10 to 14 than Jet50-Bio50. However, it has less normal alkanes with

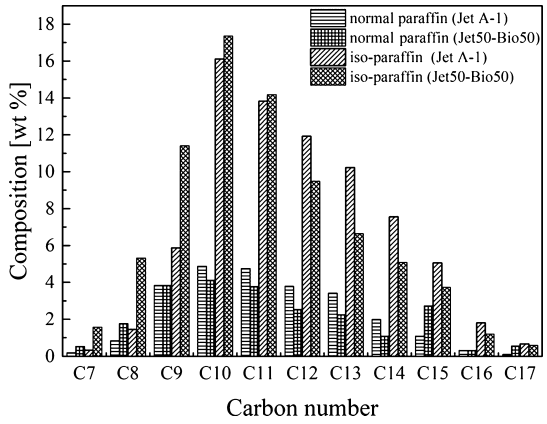

Figure 2. Carbon distribution of normal and isomerized alkanes in Jet A-1 and Jet50-Bio50.

carbon numbers from 7 to 8 and from 15 to 17. On the other hand, in terms of *iso*-alkanes, a carbon number distribution of Jet A-1 is lower than that of Jet50-Bio50 from C7 to C11, but it is higher from C12 to C17. These distinct distributions would affect the oxidation of each fuel, leading to different ignition delays from each other.

For numerical simulations of the fuel oxidation or ignition process, a real jet fuel is emulated by a surrogate fuel. The properties of a surrogate fuel should be as close to those of a real fuel as possible. For this purpose, major properties relevant to combustion characteristics are considered, which are called here as combustion property targets (CPTs).[9−13] In this work, four major properties such as H/C ratio, molecular weight, derived cetane number (DCN), and threshold soot index (TSI) are selected as CPTs to maintain the combustion characteristics of a real fuel. Laminar flame speed and the other properties (e.g., Wobbe index) are not considered in this work, where the study is focused on ignition and the initial oxidation process. The properties of the two fuels, Jet A-1 and Jet50-Bio50, are summarized in Table 1. It is found that Jet50-Bio50 has a larger molecular weight, higher DCN, and smaller TSI than Jet A-1. The molecular weight mainly affects the mass diffusion and local equivalence ratio. DCN is correlated with the ignition delay of a liquid fuel after injection into a chamber. DCN was measured according to the ASTM D6890 standard,[14] and an ignition quality tester (IQT) was used as a device to measure the ignition delay time, ID, in msec, for DCN. It is calculated by the equation

$$\mathrm{DCN} = 4.460 + \left(\frac{186.6}{\mathrm{ID}}\right) \quad (1)$$

https://doi.org/10.1021/acsomega.1c04002
ACS Omega 2021, 6, 26646−26658

Table 1. CPTs of Jet A-1 and Jet50-Bio50

Properties	fuels		
	Jet A-1	Jet50-Bio50	Bio-Jet
chemical formula	$C_{10.2}H_{20.5}$	$C_{12.3}H_{24.4}$	
H/C ratio	2.01	1.98	
molecular weight [g/mole]	143 ± 4	172 ± 5	210
DCN	46.6 ± 0.6	62 ± 0.6	
density (kg/m^3 at 15 °C)	794	786	767
flash point (°C)	38	52	66
kinematic viscosity (mm^2/s at −20 °C)	3.2	4.2	5.2
TSI (smoke point)	17.3 (25.14 mm)	10.1 (45.88 mm)	

and TSI[15,16] indicates soot propensity, which is calculated by two properties such as molecular weight (g/mol) and smoke-point (mm) length. Smoke point was measured according to the ASTM D1322 standard,[17] and from the stipulation, its highest measurable length is 50 mm. Longer smoke point means lower soot propensity. TSI is expressed in the equation

$$\mathrm{TSI} = a\left(\frac{\text{molecular weight}}{\text{smoke point}}\right) + b \tag{2}$$

where the constants, a and b, are determined from preliminary experiments. For this purpose, two distinct baseline fuels are selected in terms of smoke point and they are methylcyclohexane and 1-methylnaphthalene, which are the same as the selected ones in the previous work.[18] As a result, the two constants are determined to be 3.667 and −3.663, respectively. From eq 2, the larger value of TSI means that more smoke is generated. Accordingly, from Table 1, slower mass diffusion, shorter ignition delay, and lower sooting propensity are expected for Jet50-Bio50 than for Jet A-1.

Surrogate fuels for the two fuels are configured to make the best fit of CPTs between a real fuel and its surrogate fuel, respectively. In this study, the selected components of a surrogate fuel are *n*-hexadecane, *n*-dodecane, *iso*-octane, and 1,3,5-trimethylbenzene. These four components represent *n*-alkanes, iso-alkanes, and aromatics, respectively.[19,20] The mole fraction of each component for the two surrogate fuels is listed in Table 2, where the CPTs of the surrogated fuels are shown. As seen in the table, the CPTs of a surrogate fuel agree well with those of its real fuel in Table 1, and accordingly, both surrogate fuels would properly simulate the oxidation processes of Jet A-1 and Jet50-Bio50, respectively. From the table, the total content of *n*-alkanes such as *n*-hexadecane and *n*-dodecane in the surrogate fuel for Jet A-1 is less than that for Jet50-Bio50. Particularly, focused only on *n*-hexadecane, which is the heaviest component in the surrogate fuels, its mole fraction in the surrogate fuel for Jet A-1 is much less than that for Jet50-Bio50 because Jet50-Bio50 has a larger molecular weight than Jet A-1 by around 20%. On the other hand, the surrogate fuel for Jet A-1 has a more aromatic component 1,3,5-trimethylbenzene than Jet50-Bio50 because the bio-jet fuel adopted here does not contain any aromatics. Regarding *iso*-alkanes, they are contained more in the surrogate fuel for Jet A-1, which contradicts their relative composition of the real fuels, Jet A-1 and Jet50-Bio50, which shows more *iso*-alkanes in Jet50-Bio50 and not in Jet A-1. This is because the simultaneous fit cannot be made perfectly with these four components in terms of the four CPTs. In other words, when the molecular weight of Jet50-Bio50 is realized by the surrogate fuel with the present four components, the maximum mole fraction of *iso*-octane is limited. However, the summed mole fraction of *n*-alkanes and *iso*-alkanes in the surrogate fuels follows the tendency of the real fuels; that is, the surrogate fuel for Jet50-Bio50 has more alkanes than that for Jet A-1 by 12.5% in mole fraction. These surrogate fuels are adopted in numerical simulations in later sections.

2.2. Experimental Methods. In this study, the ignition delay of Jet A-1 and Jet50-Bio50 is measured by a shock tube adopted in our previous work.[4] Experiments are conducted at 20 atm and stoichiometric equivalence ratio. It is measured over a wide range of temperatures from 670 to 1250 K.

Concentrations of the two species, O_2 and CO, are measured by using a laminar flow reactor during the oxidation process of both fuels Jet A-1 and Jet50-Bio50. They are measured as a function of residence time of a fuel at 6 atm, 968 K, and stoichiometric equivalence ratio. Furthermore, the concentration of O_2 is demonstrated as a function of temperature over a wide range of temperatures from 550 to 950 K at a constant residence time of a fuel to see the temperature-dependent reactivity of each fuel.

2.2.1. Measurement of Ignition Delay Time by a Shock Tube. The experimental apparatus including a shock tube is shown in Figure 3.[22] The driver section is 1.45 m long and has an inner diameter of 66.9 mm, and the driven section is 5.85 m long and has an inner diameter of 64.7 mm. Details on the experimental apparatus including a shock tube can be found in the previous work.[4] The driven section itself and the feeding lines connected to the section are heated up to 150 °C. An evaporator, where liquid fuels are vaporized, is maintained at a low pressure of 1×10^{-2} Torr, and the injected fuels are completely evaporated during sufficient time to attain a steady state. Then, the driven section is depressurized to a pressure below 1×10^{-5} Torr. The evaporated fuel, the inert gas of high-purity N_2, and the oxidizer of high-purity O_2 are supplied into the driven section, consecutively. The fuel, N_2, and O_2 are mixed homogeneously in the driven section for a longer time than 12 h.

Next, the driver section is filled with high-purity He and N_2, whose composition satisfies a tailored condition. When gases between double diaphragms are evacuated, the diaphragms burst abruptly by the pressure difference between the driver and the driven sections. Therefore, a shock wave is generated and propagates into the driven section. Four pressure transducers (model PCB 112B05) are installed in an axial direction along the driven section to determine the propagation velocity of a shock wave. From the velocity of the reflected shock wave at the end wall, the gas temperature behind the reflected shock wave is calculated. The uncertainty limit of the temperature is ±20 K, and it leads to the uncertainty of 20% in ignition delay.[21,22] At the end wall, a pressure transducer (model Kistler 603C) and a

Table 2. Mixture Mole Fraction and CPTs of the Surrogate Fuels Suggested for Jet A-1 and Jet50-Bio50

	normal hexadecane	normal dodecane	*iso*-octane	1,3,5-trimethyl benzene	H/C	MW [g/mole]	DCN	TSI
Jet A-1	0.05	0.405	0.300	0.245	2.004	143.8	50.5	20.7
Jet50-Bio50	0.380	0.240	0.229	0.151	2.065	170.9	65.9	15.0

https://doi.org/10.1021/acsomega.1c04002
ACS Omega 2021, 6, 26646−26658

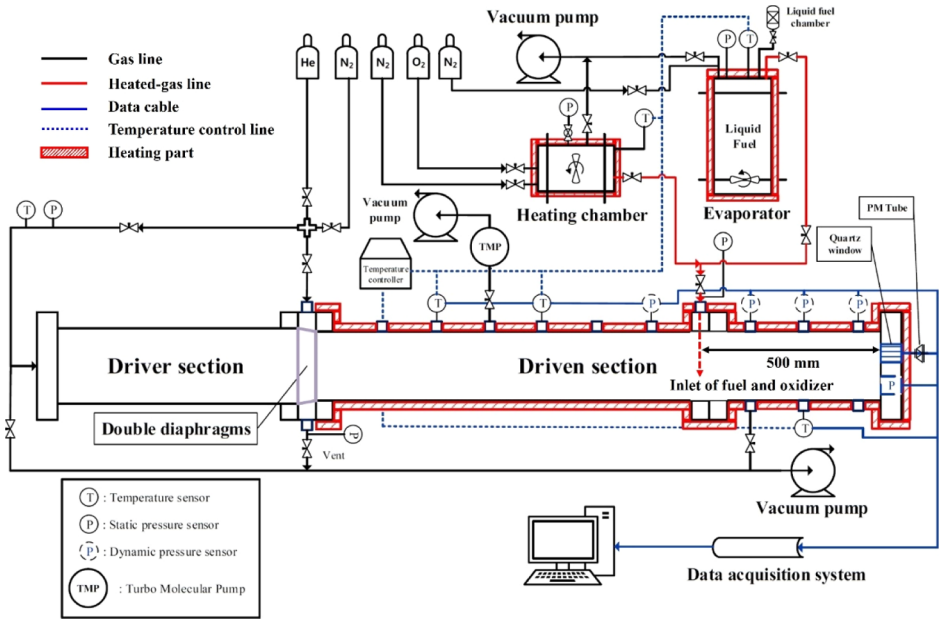

Figure 3. Schematic diagram of the shock tube for the measurement of ignition delay time.

quartz window are installed to measure the pressure behind a reflected shock wave and for the optical access of a photomultiplier tube (PMT), respectively. The intensity of chemiluminescence from a CH* radical with a wavelength of 431 ± 1 nm is measured by a PMT, and it indicates the reaction progress during the ignition process.

Inevitable pressure rise before complete ignition inside the driven section is induced by the well-known boundary layer effect, and it is evaluated by the normalized parameter, $(1/P)(dP/dt)$, which should be maintained low around 3.5%/ms.[4] The two fuels Jet A-1/O_2/N_2(1.35/20.73/77.92 mol %) and Jet50-Bio50/O_2/N_2(1.13/20.77/78.10 mol %) are tested in the present experiments. Thermodynamic and flow conditions for experiments with the two jet fuels are summarized in Table 3.

Table 3. Thermodynamic and Flow Conditions for Numerical Simulations of Ignition Delay in a Shock Tube

	fuel	
variables or parameters	Jet A-1	Jet50-Bio50
pressure [atm]	20	20
temperature [K]	650−1250	650−1250
equivalence ratio	1	1
fuel [%]	1.345	1.127
O_2 [%]	20.726	20.772
N_2 [%]	77.929	78.101

2.2.2. Measurement of Species Concentrations by a Laminar Flow Reactor. In a laminar flow reactor shown in Figure 4, its wall temperature is maintained constant and chemical reaction of the mixture occurs herein. The fuel−oxygen mixture flows through the reactor vessel, and at the same time, the fuel is oxidated gradually. In front of the reactor, an evaporator and a preheater are installed in order to vaporize the liquid fuel and to rapidly raise the temperature of the mixture to a specified temperature, respectively. A liquid fuel and nitrogen gas enter the evaporator and come out as a gaseous mixture (evaporated fuel + nitrogen gas), as shown in Figure 4. Then, it is mixed with oxygen to attain the equivalence ratio of the

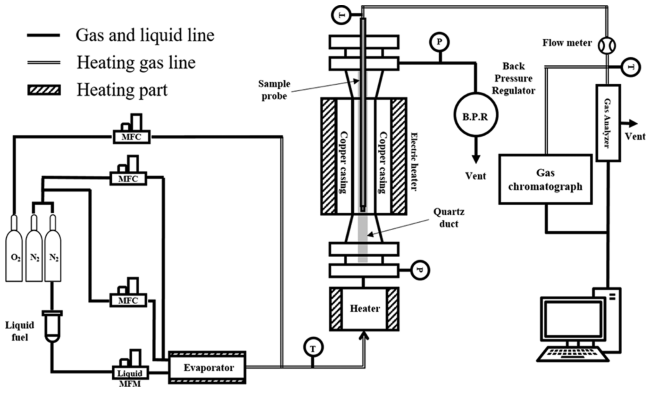

Figure 4. Schematic diagram of the experimental apparatus (laminar flow reactor).

experimental conditions and enters the heater for preheating. The length of the reaction zone in the reactor is 1200 mm, and a quartz duct with an inner diameter of 10 mm is installed concentrically inside the reactor. A sample probe is mounted at the top of the reactor and inserted into the quartz duct downward to extract a product gas. It moves downward and upward to locate its position axially. The position is correlated with the residence time of the mixture in the reactor; that is, the residence time can be calculated by the axial position of the sample probe and the mean velocity of the mixture. The reactor is surrounded by a copper casing to make the wall temperature of the reactor uniform in an axial direction. Moreover, the casing is surrounded by electric heaters which are composed of four pieces to maintain the wall temperature of the reactor at a specified constant in the axial direction. At the downstream of the reactor, a back pressure regulator is installed to adjust the operating pressure. In the measurement part, the concentration of a product gas coming through the sample probe is measured. The part is heated and insulated by a heating cable to prevent the gas from being condensed. Two main species of O_2 and CO are selected to see the reactant consumption and product-gas production, respectively. Their concentrations are measured by

https://doi.org/10.1021/acsomega.1c04002
ACS Omega 2021, 6, 26646−26658

using gas chromatography, and the data are stored in a computer.

Experiments with a flow reactor are conducted by two methods. At first, concentrations of chemical species in the product gas are measured at a specified pressure and reactor-wall temperature as a function of residence time, which is variable by changing the position of a sample probe. In the second method, concentrations are measured at a specified pressure and residence time as a function of temperature. From this measurement, the global reactivity of a fuel in its oxidation process can be evaluated over a wide range of temperatures.

Thermodynamic and flow conditions for experiments with the two jet fuels are summarized in Table 4. As can be seen in the table, experiments are conducted at 6 atm and unity equivalence ratio with the same carbon concentration of 0.3% for both fuels. Variable parameters are residence time and temperature in the two methods, respectively. The residence time variable is changed from 0.125 to 2.0 s. Moreover, global-reactivity experiments with temperature variable are conducted at a constant residence time of 2.0 s and at temperatures ranging from 550 to 950 K with a step of 50 K interval. Additionally, the experiment is conducted at 968 K, which is the allowable highest temperature with a uniform temperature profile attained axially in the present reactor. In this experiment, it was impossible to make the axial temperature uniform due to heat loss to the surroundings at high temperatures over 968 K. Below the critical temperature, uniform temperatures are attained and temperature profiles are shown at various temperatures in Figure 5. Axial deviation in temperature is within ±5 K, which is comparable with that reported in previous works.[23−25]

Table 4. Thermodynamic and Flow Conditions for Experiments and Numerical Simulations with a Laminar Flow Reactor

	Fuel	
variables or parameters	Jet A-1	Jet50-Bio50
pressure [atm]	6	6
temperature [K]	550−968	550−968
residence time [s]	0.125−2.0	0.125−2.0
equivalence ratio	1	1
oxidizer	oxygen	oxygen
fuel [%]	0.031	0.037

In Figure 5, the distance of 0 mm indicates the origin point which is the bottom of the reactor. The electric heater starts heating from the point and ends at 1200 mm. The reactor-wall temperature rises from 500 to 950 K and finally up to the highest temperature of 968 K. Thermal equilibrium is attained between gases inside the reactor and the reactor wall. From the temperature profiles shown in Figure 5, available lengths for experiments are found, which depend moderately on the temperature and range from 550 to 800 mm. The higher the temperature is, the shorter the available length becomes. Axial uniformity of the temperature along the reactor is satisfactory.

2.3. Kinetic Model and Conditions for Numerical Simulations. For numerical simulations, a detailed chemical kinetic model[22] for a real jet fuel is adopted here, and it was developed from the first- and second-generation surrogate fuels validated by Dooley et al.[10] and Malewicki et al.[20] The kinetic model is based on the core mechanism for the $C_0−C_4$ chemistry developed by Metcalfe et al.,[27] and then, the core mechanism is combined with the individual kinetic models for *iso*-octane, 1,3,5-trimethylbenzene, and *n*-dodecane and *n*-hexadecane developed by Mehl et al.,[28] Gudiyella and Brezinsky,[29] and Westbrook et al.,[19] respectively. The constructed detailed model is composed of 3147 species and 12,448 reaction steps.[26]

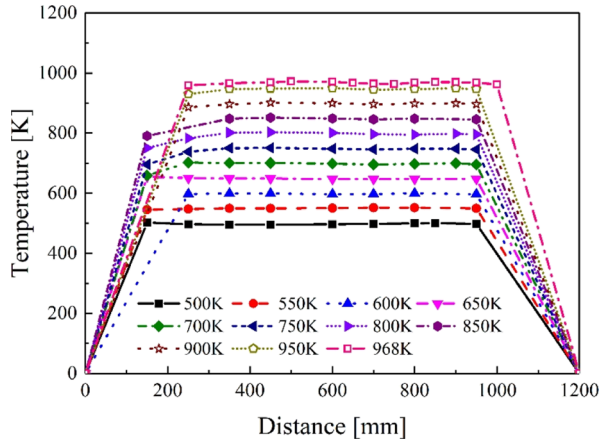

Figure 5. Temperature profiles measured along the reactor tube within a reaction zone of 1200 mm.

Measured data by the shock tube and the flow reactor in this work are compared with numerical predictions in terms of ignition delay and oxidation process, respectively. For this purpose, numerical simulations are conducted by using the well-known program package of the Chemkin-Pro.[30] Ignition delay of a mixture is calculated with a closed homogeneous reactor model and the oxidation process is calculated with the plug-flow reactor (PFR) model. Based on the numerical results, reaction pathways for the oxidation of each fuel are analyzed. For numerical simulations, the surrogate fuels for Jet A-1 and Jet50-Bio50 in Table 2 are adopted with the aforementioned detailed chemistry.[26,31] Thermodynamic and flow conditions for the calculations of ignition delay and oxidation are summarized in Tables 3 and 4, respectively.

3. RESULTS AND DISCUSSION

3.1. Ignition Delay Time. Ignition delay times are measured and calculated at 20 atm and unity equivalence ratio for the two jet fuels Jet A-1 and Jet50-Bio50, which are demonstrated in Figure 6. Both fuels show negative temperature coefficient (NTC) behavior[4] in the similar temperature range. Numerical results agree well with experimental data in a qualitative manner. However, at low temperatures below 750 K, numerical simulations cannot follow the significant quantitative difference between the ignition delays of Jet A-1 and Jet50-Bio50 observed in experiments. It is because the present chemical mechanism does not reflect the low-temperature chemistry of a jet fuel accurately.

It is notable that Jet50-Bio50 has an appreciably shorter ignition delay than Jet A-1 at temperatures below 1000 K, while ignition delays of both fuels are almost the same as each other at higher temperatures. It implies that the reaction or breakdown of Jet50-Bio50 is initiated earlier and activated more than Jet A-1 at low temperatures, where it takes a relatively longer time than at high temperatures. From experimental data, the largest difference in ignition delay between the two fuels is 228%. It is found that the ignition of Jet50-Bio50 is accelerated much faster than that of Jet A-1 and more *n*-alkanes in Jet50-Bio50 contribute to this acceleration at low temperatures. It will be discussed in the next section in more detail.

https://doi.org/10.1021/acsomega.1c04002
ACS Omega 2021, 6, 26646−26658

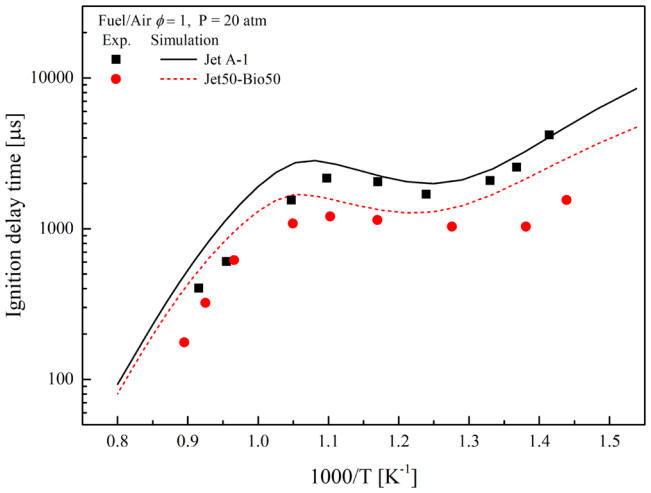

Figure 6. Ignition delay times of Jet A-1/air and Jet50-Bio50/air over a wide range of temperatures. Points indicate experimental data (square symbols: Jet A-1, circle symbols: Jet50-Bio50) and lines indicate model predictions (straight line: Jet A-1, dotted line: Jet50-Bio50).

3.2. Oxidation Process and Reaction Pathway. As aforementioned, the oxidation process is investigated intensively by experiments with the flow reactor and simulations with the PFR model, which provides information on the global reactivity of the two fuels. First, concentrations of O_2 and CO in a product gas are measured and calculated as a function of residence time of the mixture by changing the position of the sample probe. Concentration profiles at 950 K are demonstrated in Figure 7 over the range of residence time from 0.125 to 2.0 s for Jet A-1 and Jet50-Bio50, respectively.

Although there are quantitative discrepancies between experimental and numerical data in Figure 7, both data show that the O_2 concentration decreases more gradually in Jet A-1 than in Jet50-Bio50. This means that the reactivity of Jet A-1 is relatively smaller than that of Jet50-Bio50. Similarly, the concentration of CO in Jet50-Bio50 rises more rapidly than that in Jet A-1. Furthermore, it is seen that the concentration of CO in Jet50-Bio50 is always higher than that in Jet A-1 at any residence time.

Numerical results show the same behaviors in the relative reactivity of both fuels but more appreciably; that is, the concentration of O_2 in Jet A-1 maintains the initial value and then slightly decreases from 0.3 s until around 0.8 s. However, its concentration in Jet50-Bio50 decreases rapidly after 0.3 s. On the other hand, a product, CO, is produced gradually as the reaction progresses and then increases rapidly. The concentration of CO in Jet50-Bio50 is higher at all times than that in Jet A-1, and it increases more rapidly. From these results, it can be seen that Jet50-Bio50 is more reactive than Jet A-1 at the same residence time.

From experiments and numerical simulations, concentrations of O_2 in the two fuels at a specified residence time of 2.0 s are measured and calculated as a function of temperature, and they are shown in Figure 8, which imply the global reactivity of the fuels. These results confirm that the difference in reactivity between Jet A-1 and Jet50-Bio50 is more significant at a lower temperature; that is, the concentration of O_2 in Jet A-1 is almost unchanged up to 570 K and then slightly decreases up to 600 K. At temperatures between 600 and 750 K, NTC behavior is observed in simulations but not clearly in experiments. At higher temperatures above 750 K, oxygen is consumed moderately

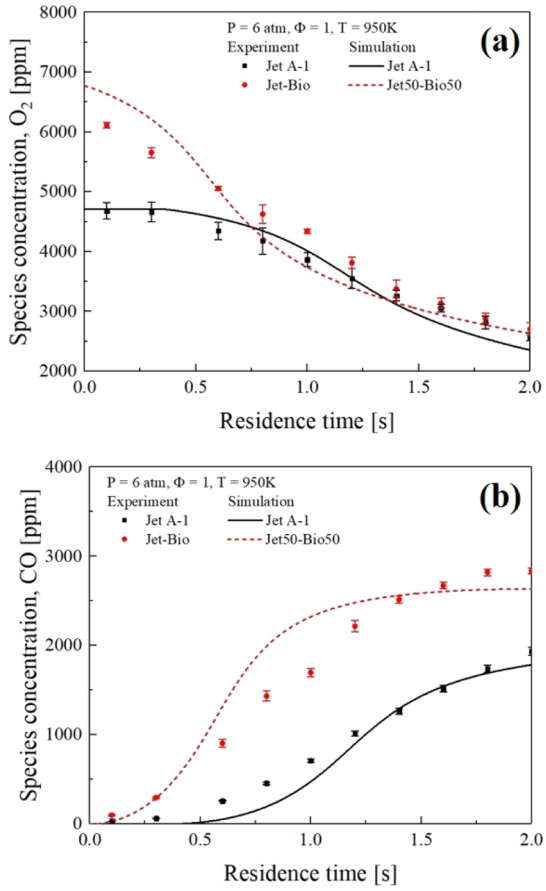

Figure 7. Concentration profiles of (a) O_2 and (b) CO measured as a function of time in the flow reactor at 6 atm, 0.3% carbon, equivalence ratio, Φ = 1.0, and T = 968 K (symbols: experimental data, lines: model predictions) expressed with time shifts of +0.35 and +0.29 s for Jet A-1 and Jet50-Bio50, respectively.

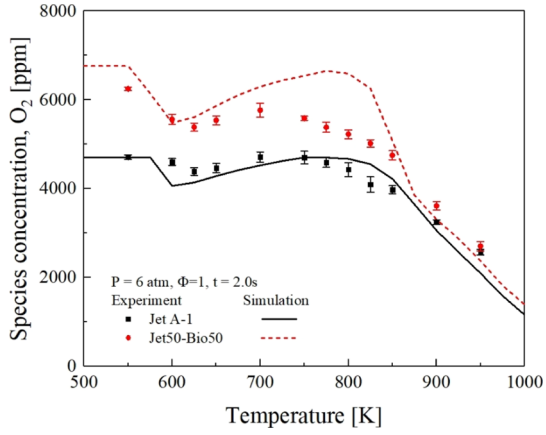

Figure 8. Concentration of O_2 as a function of temperature indicating the global reactivity of two fuels at 6 atm, 0.3% carbon, Φ = 1.0, and residence time, t = 2.0 s (symbols: experimental data, lines: model predictions).

again and rapidly over 850 K. From this global reactivity of O_2, it is found that the reaction of Jet A-1 is initiated at around 570 K. The overall behavior in Jet50-Bio50 is similar to that in Jet A-1, but it is notable that the reaction of Jet50-Bio50 starts at a lower temperature than that of Jet A-1 or at around 550 K, which means that Jet50-Bio50 is more reactive than Jet A-1 at low

https://doi.org/10.1021/acsomega.1c04002
ACS Omega 2021, 6, 26646−26658

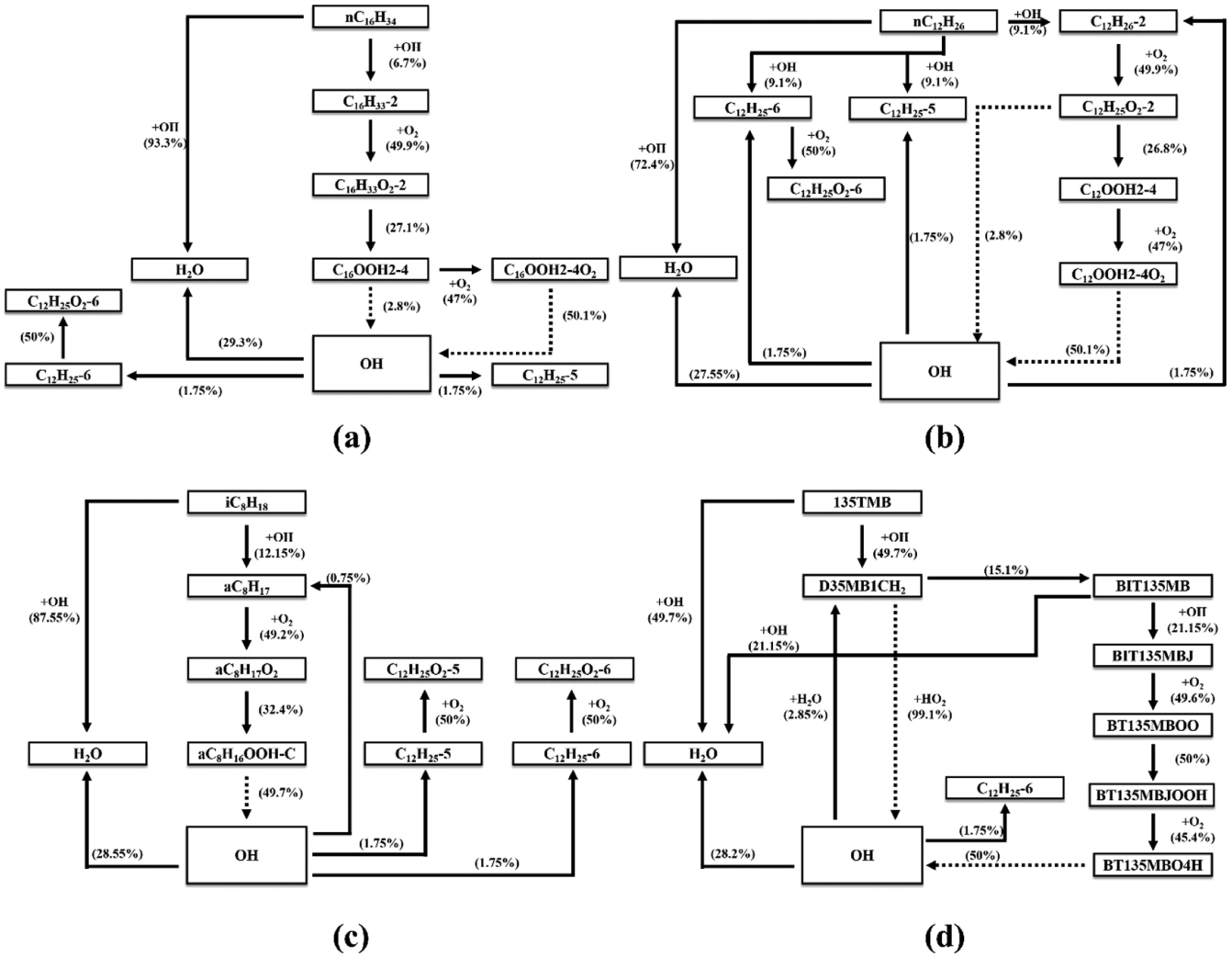

Figure 9. Reaction pathways for the oxidation of Jet A-1 at 6 atm, Φ = 1.0, and T = 600 K: (a) *n*-hexadecane, (b) *n*-dodecane, (c) *iso*-octane, and (d) 1,3,5-trimethylbenzene (dotted arrows indicate the formation reaction of OH species).

temperatures. At high temperatures over 900 K, the slopes of concentration in both fuels are almost the same as each other. This reactivity dependence on temperature in both fuels agrees well with the dependence of ignition delay time on temperature, as shown in Figure 6. Accordingly, Jet50-Bio50 has an earlier ignition and higher reactivity at low temperatures below 900 K. However, both Jet50-Bio50 and Jet A-1 have the same reactivity at high temperatures over 900 K.

Reactivity dependence of Jet50-Bio50 on a temperature different from that of Jet A-1 found in Figure 8 would result from its reaction pathways distinct from those of Jet A-1. Accordingly, reaction pathways relevant to the reaction of four major surrogate components, *n*-hexadecane, *n*-dodecane, *iso*-octane, and 1,3,5-trimethylbenzene denoted by *n*-$C_{16}H_{34}$, *n*-$C_{12}H_{26}$, *i*-C_8H_{18}, and 135TMB, respectively, are investigated here at both low and high temperatures. The present analysis is conducted based on reactions in the PFR model. The two temperatures are selected as 600 and 1100 K, respectively.

For the analysis, reaction pathways dedicated to the generation of OH species are investigated because it is one of the critical radicals that affect the initiation of the chain-branching reaction. Here, the reaction starts with each surrogate component and the final species is the OH radical. The reaction pathways of the two fuels at low temperatures are shown in Figures 9 and 10, respectively. The dotted arrows in the figures indicate the pathways relevant to the production of OH. From Figures 9 and 10, it is found that all the reaction pathways are simple and proceed straightforward with a weak coupling of a species with a small number of the other species. Contribution of the other reactive radicals such as H and O to OH production is negligible. Moreover, the reaction pathway of each surrogate component in Jet A-1 is significantly different from that in Jet50-Bio50 in terms of intermediate species and relative weight in producing the OH radical. Interestingly, the reaction pathways of *n*-$C_{12}H_{26}$ in Jet A-1 and *n*-$C_{16}H_{34}$ of Jet50-Bio50 are similar to each other. It is because *n*-$C_{12}H_{26}$ in Jet A-1 and *n*-$C_{16}H_{34}$ in Jet50-Bio50 are the heaviest and major components, respectively, as listed in Table 2, and they contribute mainly to breakdown reaction into various lighter hydrocarbons than *n*-$C_{12}H_{26}$ or *n*-$C_{16}H_{34}$. Especially, the reaction of 135TMB is relatively weak at low temperatures,[32] and its reaction pathways for the two fuels are quite different from each other, as shown in Figures 9d and 10d. The OH radical is produced through more various pathways from 135TMB in Jet50-Bio50.

On the other hand, reaction pathways of the same components at a high temperature of 1100 K are illustrated in Figure 11, which are for Jet A-1. Compared with reaction pathways at low temperatures, they are much more complex, and

https://doi.org/10.1021/acsomega.1c04002
ACS Omega 2021, 6, 26646−26658

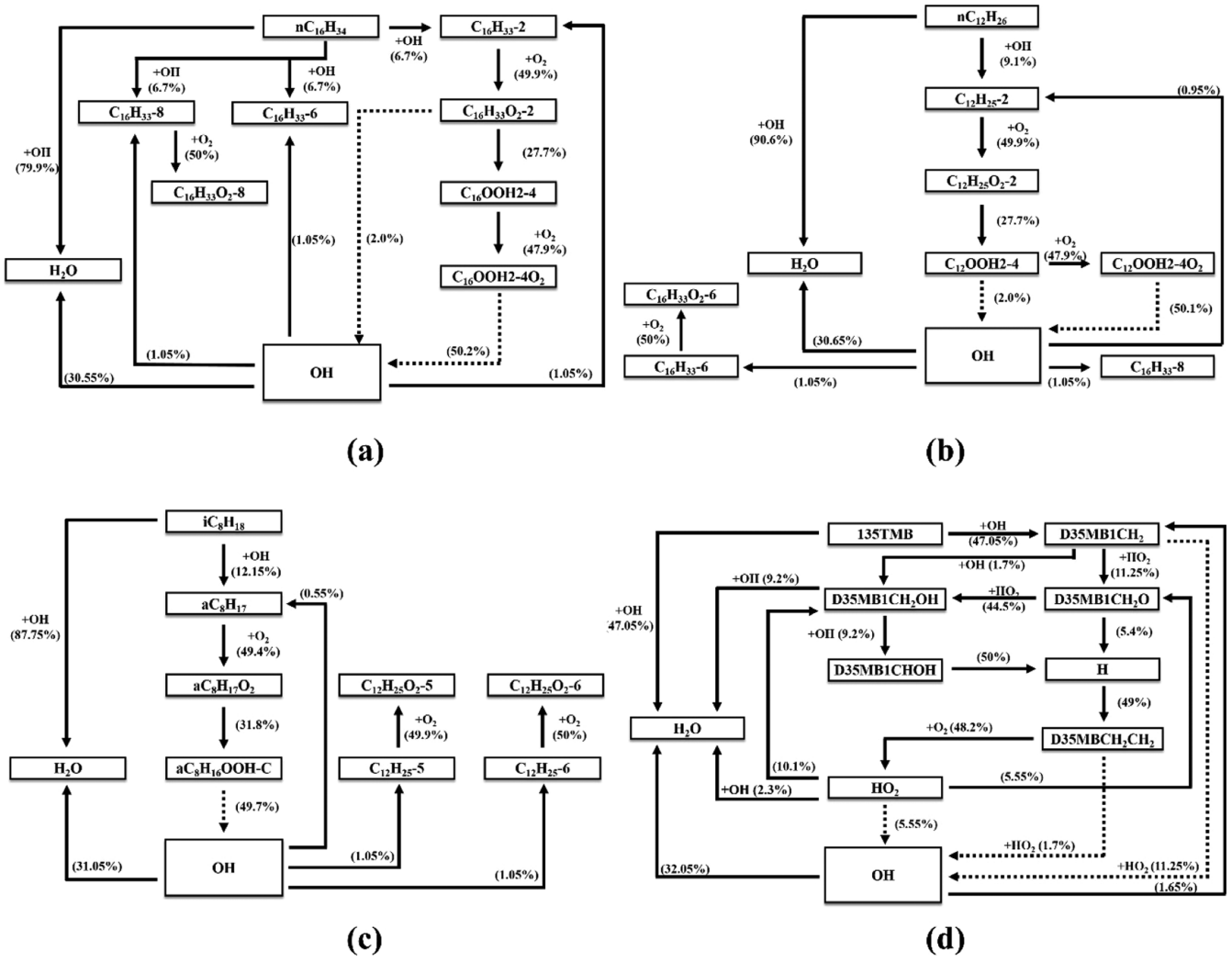

Figure 10. Reaction pathways for the oxidation of Jet50-Bio50 at 6 atm, Φ = 1.0, and T = 600 K: (a) *n*-hexadecane, (b) *n*-dodecane, (c) *iso*-octane, and (d) 1,3,5-trimethylbenzene (dotted arrows indicate the formation reaction of OH species).

a species is connected with a larger number of the other species by multiple coupling. Furthermore, various reactive radicals such as H and O are involved in producing the OH radical as the intermediate species. In these aspects, reaction pathways at high temperatures are completely different from those at a low temperature of 600 K, as shown in Figures 9 and 10. They show the typical reactions of high-temperature chemistry controlled by chain-branching reactions with a large activation energy. At high temperatures, reaction pathways in Jet50-Bio50 are almost the same as those in Jet A-1 in all the aspects, and the pathway diagram for Jet50-Bio50 is omitted here.

As aforementioned, reaction pathways of both fuels at a low temperature are significantly different from each other. Accordingly, they would make different reaction kinetics, which should result in a difference in the transient speciation profiles of major reactants and radicals. Concentration profiles of three species, OH, *n*-$C_{16}H_{34}$, and 135TMB, are calculated as a function of time with the PFR model at low and high temperatures and shown in Figure 12. At a low temperature of 600 K, the OH radical in Jet50-Bio50 is produced significantly earlier than in Jet A-1 by around 0.5 s, and its concentration increases more rapidly with a higher peak than in Jet A-1. On the other hand, at a high temperature of 1100 K, it is produced still earlier than in Jet A-1, but the interval between them is slight, which is only 0.1 s, and the peaks of OH concentration in both fuels are comparable with each other. Concentrations of the major components, *n*-$C_{16}H_{34}$ and 135TMB, show consumption of the species in Figure 12.

The two components, *n*-$C_{16}H_{34}$ and 135TMB, are selected because they are a representative *n*-alkane and an aromatic compound, respectively. At low temperatures, they are consumed much earlier in Jet50-Bio50 than in Jet A-1 as the OH radical is produced earlier in Jet50-Bio50. Moreover, their slow consumption lasts for a long time of around 0.5 s for *n*-$C_{16}H_{34}$.

However, at high temperatures, they are consumed at the almost same time and rapidly in both fuels. Moreover, the duration of consumption is short, which is 0.01−0.1 s. Regarding the consumption of 135TMB, it is consumed out in a short time at a high temperature, while it still remains for a long time at a low temperature. Accordingly, it is found that Jet50-Bio50 has different kinetics from Jet A-1, and it has a relatively high low-temperature reactivity. On the other hand, at high temperatures, the reaction is so fast that there is little difference between the reactivity of both fuels.

In addition to the transient concentration profiles of several species, the production rates of several elementary reaction steps relevant to OH generation, especially shown in reaction

https://doi.org/10.1021/acsomega.1c04002
ACS Omega 2021, 6, 26646−26658

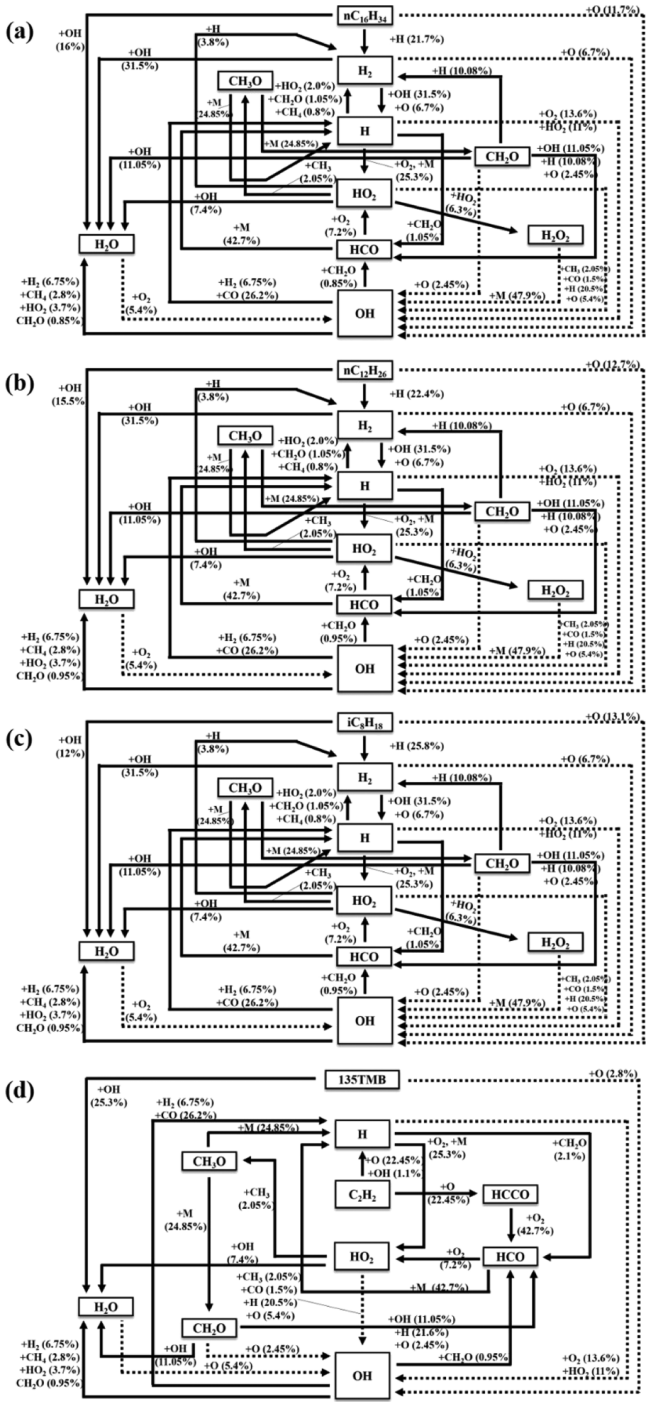

Figure 11. Reaction pathways for the oxidation of Jet A-1 at 6 atm, Φ = 1.0, and T = 1100 K: (a) *n*-hexadecane, (b) *n*-dodecane, (c) *iso*-octane, and (d) 1,3,5-trimethylbenzene (dotted arrows indicate the formation reaction of OH species).

pathways in Figures 9, 10, and 11, are calculated as a function of time and shown in Figure 13. At low temperatures, Figure 13a–d presents the production rates of the principal reaction steps in each pathway of *n*-$C_{16}H_{34}$, *n*-$C_{12}H_{26}$, *i*-C_8H_{18}, and 135TMB, respectively. It is found that OH is produced mainly through the breakdown reaction of heavy hydrocarbon components with a high carbon number. From their production rates, all the reaction steps in Jet50-Bio50 are initiated at around 0.5 s and significantly earlier than in Jet A-1 by around 0.5 s. Furthermore, their peaks in Jet50-Bio50 are higher, and especially, the reaction from the pathway of *n*-$C_{16}H_{34}$ has a large difference in the peak of the production rate between the two fuels. It is because Jet50-Bio50 contains more *n*-$C_{16}H_{34}$ than Jet A-1, as shown in Table 2. On the other hand, at high temperatures, Figure 13e–h presents the production rates of the principal reaction steps in each pathway of the four surrogate components, respectively. At high temperatures, chain-branching reactions are activated appreciably and well-known hydrogen–oxygen shuffle reactions are dominant in producing the OH radical. From Figure 13h, it is found that the oxidation of light components from 135TMB contributes to OH generation rather than that of heavier components. Even at a high temperature, all the reaction steps in Jet50-Bio50 are initiated earlier than Jet A-1, but the initiation time is around 0.1–0.2 s, which is much shorter than at low temperatures. Furthermore, the difference between initiation times of the two fuels is significantly small compared with that at low temperatures. Still, their peaks in Jet50-Bio50 are also higher at high temperatures as observed at low temperatures, but the reaction from the pathway of *n*-$C_{16}H_{34}$ does not show very large difference in the peak of the production rate between the two fuels, as shown in Figure 13a at a low temperature. It implies the high reactivity of all the components irrespective of fuel components at high temperature and dominance of high-temperature chemistry with strong dependence of reactions on the temperature. These results show a good agreement with those in Figure 12 in terms of reaction initiation and reactivity. Although not shown here, the rate of production of the OH radical showed the same behaviors as in Figure 13.

Chemical aspects of the two fuels shown in Figures 9, 10, 11, 12, and 13 are summarized here. Both jet fuels have simple reaction pathways at low temperatures, although they are distinctive from each other. However, Jet50-Bio50 has a stronger reactivity in the reaction pathways of *n*-hexadecane with the largest molecular weight than Jet A-1; that is, the alkylperoxy radical isomerization,[19] which affects low-temperature reactivity, is enhanced by the species with a large molecular weight. During the breakdown of a fuel, heavy hydrocarbons are converted into light ones. Accordingly, Jet50-Bio50 with a larger molecular weight produces more various radicals and its reactions are initiated earlier. Consecutively, reactions of 1,3,5-trimethylbenzene are more enhanced by more radicals produced from Jet50-Bio50. It enables the earlier ignition of Jet50-Bio50 than Jet A-1, especially at low temperatures. This phenomenon still works even at high temperatures. However, reactions are fast enough to make the major components decompose and the radical produce within a short time. Moreover, typical chain-branching reactions are dominant in the initiation of reactions. Accordingly, both fuels show the almost same reaction kinetics and pathways, leading to the same ignition delay as the other fuel.

3.3. Low-Temperature Ignition Propensity Observed by the CH_2 Functional Group. Dussan et al.[33] suggested that the CH_2 functional group should strongly affect the chemical reaction at a low temperature. In their works, DCN was estimated by constructing surrogate fuels through the quantitative structure–property relationship (QSPR) method.[34−37] In the QSPR method, the spectrum of the overall molecular structure of a real fuel is identified by several specific chemical functional groups, and the nuclear magnetic resonator (NMR) device is used to quantify each chemical functional group reflecting the chemical structure of the fuel. Finally, its surrogate fuel is constructed by adjusting mole fractions of the surrogate-fuel components to make the surrogate fuel have the

https://doi.org/10.1021/acsomega.1c04002
ACS Omega 2021, 6, 26646−26658

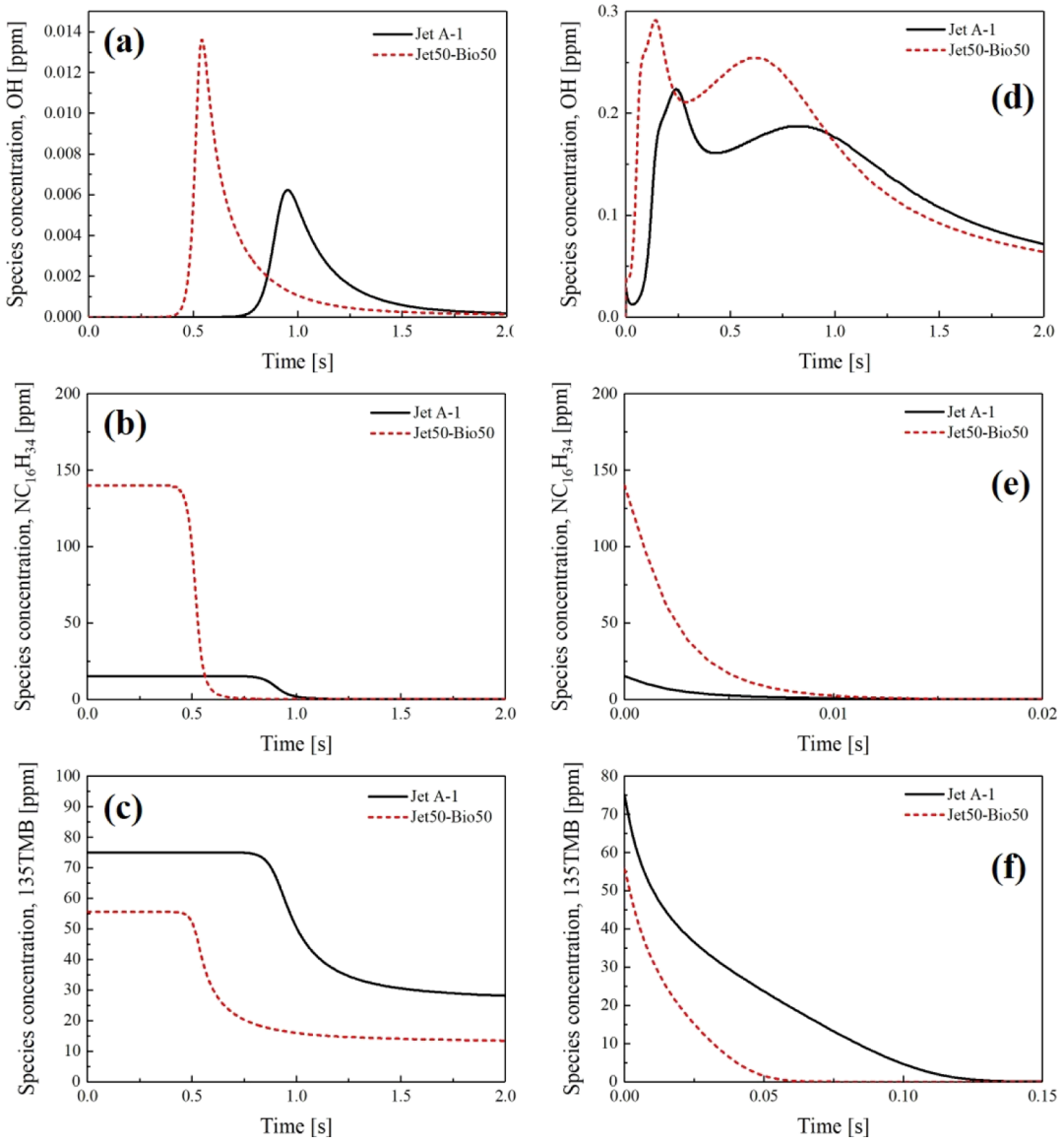

Figure 12. Transient concentration profiles of OH, $nC_{16}H_{34}$, and 135TMB calculated for Jet A-1 and Jet50-Bio50 as a function of time at 6 atm, 0.3% carbon, $\Phi = 1.0$, and at low and high temperatures [(a) OH, (b) $NC_{16}H_{34}$, (c) 135TMB at $T = 600$ K and (d) OH, (e) $NC_{16}H_{34}$, and (f) 135TMB at $T = 1100$ K].

same functional groups as the real fuel. Typical chemical functional groups selected for this purpose are CH_2, CH_3, and benzyl groups. The CH_2 group represents the content of linear paraffinic components in jet fuels, while the CH_3 and the benzyl groups represent branched paraffinic and aromatic components,[33] respectively.

It is well known that the formation of QOOH, called alkylhydroperoxy radicals, is strongly influenced by the CH_2 group. Therefore, when the concentration of species belonging to the CH_2 group increases, chain branching is more probable at a low temperature, which implies that the CH_2 group comes into play more in low-temperature chemistry.[33] Earlier ignition of Jet50-Bio50 than Jet A-1 at a low temperature can be explained by applying the concept of the chemical functional group. From Figure 1, the normal alkanes amount to 26−31% in Jet A-1 and to 30−40% in bio-jet. In terms of isomerized alkanes, Jet A-1 and bio-jet have 23−29 and 60−70%, respectively. Here, isomerized alkanes are assumed to be 2-methyl groups. Then, the fraction of the molecular structure categorized into the CH_2 group in Jet A-1 is much smaller than in Jet50-Bio50. From these results, it is expected that Jet A-1 has less chain branching and slower ignition at low temperatures than Jet50-Bio50.

4. CONCLUSIONS

Ignition delay time and oxidation of the mixture fuel of Jet A-1 and a bio-jet fuel have been investigated by experiments and numerical simulations for a comparative study with a conventional jet fuel of Jet A-1. Ignition delay has been measured in a shock tube, and species concentrations in the oxidation process have been measured in a laminar flow reactor. Surrogate fuels for two real fuels of Jet A-1 and the mixture fuel, called Jet50-Bio50 here, have been constructed for numerical simulations.

Jet50-Bio50 contains more normal and isomerized alkanes than Jet A-1 because bio-jet is composed of only alkanes without aromatic compounds. From experimental and numerical results, it is found that Jet50-Bio50 has a shorter ignition delay than Jet A-1. Moreover, the difference in ignition delay is magnified as the temperature decreases. The experimental results in a laminar

https://doi.org/10.1021/acsomega.1c04002
ACS Omega 2021, 6, 26646−26658

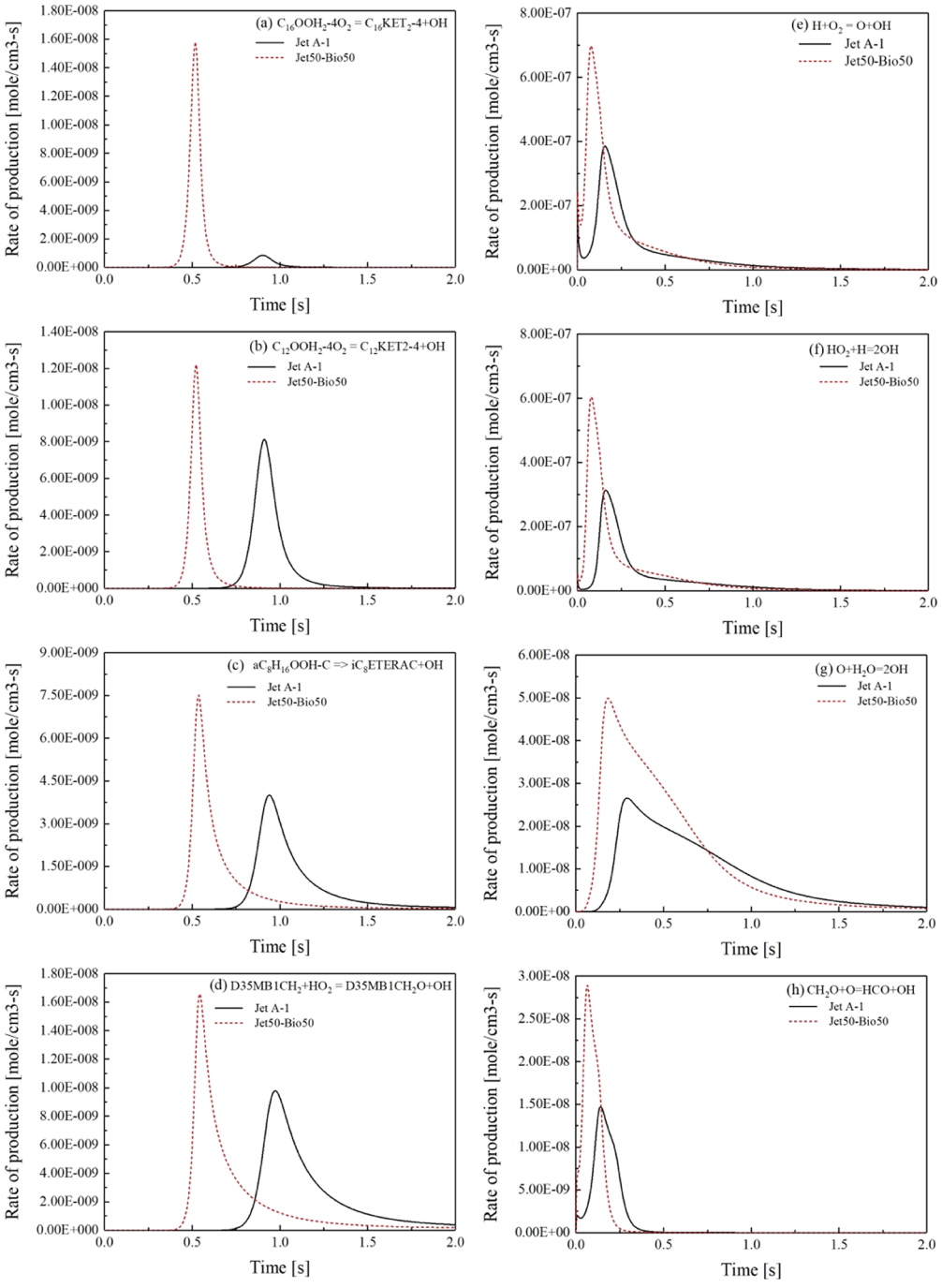

Figure 13. Production rates of several elementary reactions calculated for Jet A-1 and Jet50-Bio50 as a function of time at 6 atm, 0.3% carbon, Φ = 1.0, and at low and high temperatures [(a) $C_{16}OOH_2-4O_2$ = $C_{16}KET_2$-4 + OH at 600 K, (b) $C_{12}OOH_2-4O_2$ = $C_{12}KET_2$-4 + OH at 600 K, (c) $aC_8H_{16}OOH-C \rightarrow iC_8ETERAC$ + OH at 600 K, and (d) D35MB1CH_2 + HO_2 = D35MB1CH_2O + OH at 600 K and (e) H + O_2 = O + OH at 1100 K, (f) HO_2 + H = 2OH at 1100 K, (g) O + H_2O = 2OH at 1100 K, and (h) CH_2O + O = HCO + OH at 1100 K].

flow reactor show that Jet50-Bio50 is more reactive at the same residence time and shows a higher reactivity at low temperatures than Jet A-1, which implies that oxidation reactions are initiated at lower temperatures in Jet50-Bio50 than in Jet A-1.

Reaction pathways at low temperatures are relatively simple in both fuels at low temperature than at high temperature. Detailed pathways are distinctive in each fuel at low temperatures, while they are almost the same at high temperatures. The major surrogate components are consumed earlier and the radicals are produced earlier in Jet50-Bio50. The difference between initiation times of the two fuels is significantly larger at low temperature than at high temperature. Production rates of several reaction steps relevant to OH generation show the similar behaviors; that is, the rates in Jet50-Bio50 at low temperatures increases much earlier than in Jet A-1. On the other hand, at high temperatures, reaction pathways are relatively complex and each species is strongly coupled with the other ones through various elementary reactions. Oxidation is initiated more shortly, and the difference between the two fuels is small in terms of transient concentration profiles and initiation time of reaction. Earlier ignition and oxidation of Jet50-Bio50 at low temperatures are originated from the earlier

https://doi.org/10.1021/acsomega.1c04002
ACS Omega 2021, 6, 26646−26658

breakdown reaction of heavy alkanes than in Jet A-1 because Jet50-Bio50 has more composition of alkanes, more specifically, categorized into the CH_2 functional group, which has high reactivity at low temperatures.

Conclusively, the mixture fuel of Jet A-1 and a bio-jet fuel has earlier ignition and is more reactive at low temperatures compared with conventional jet aviation fuels. These characteristics should be considered when the blending ratio of a bio-jet fuel to Jet A-1 is determined in manufacturing alternative fuels. Furthermore, optimization of an alternative fuel would be required to fit for a jet engine combustor in terms of ignition, propulsion performance, and emission. More species should be studied by the flow reactor and the existing mechanism needs to be improved, especially at low temperatures. They will be considered as a future work for the manufacture of applicable and alternative jet fuels.

AUTHOR INFORMATION

Corresponding Author

Chae Hoon Sohn − *Department of Mechanical Engineering, Sejong University, Seoul 05006, Republic of Korea;* orcid.org/0000-0001-9836-5865; Email: chsohn@sejong.ac.kr

Authors

Cheon Hyeon Cho − *Department of Mechanical Engineering, Sejong University, Seoul 05006, Republic of Korea*

Hee Sun Han − *Department of Mechanical Engineering, Sejong University, Seoul 05006, Republic of Korea*

Jeong Sik Han − *Agency for Defense Development, Daejeon 305-600, Republic of Korea*

Complete contact information is available at: https://pubs.acs.org/10.1021/acsomega.1c04002

Notes

The authors declare no competing financial interest.

ACKNOWLEDGMENTS

This work was supported by the Agency for Defense Development of Korea under the contract UD150039GD. H.S.H. and C.H.S. were also supported by Korea Institute of Energy Technology Evaluation and Planning (KETEP) grant funded by the Korea government (MOTIE) (20206710100030, Development of Eco-friendly GT Combustor for 300MWe-class High-efficiency Power Generation with 50% Hydrogen Co-firing).

REFERENCES

(1) Yang, J.; Xin, Z.; He, Q.; Corscadden, K.; Niu, H. An overview on performance characteristics of bio-jet fuels. *Fuel* **2019**, *237*, 916−936.

(2) Wei, H.; Liu, W.; Chen, X.; Yang, Q.; Li, J.; Chen, H. Renewable bio-jet fuel production for aviation: A review. *Fuel* **2019**, *254*, 115599.

(3) Pavlenko, N.; Kharina, A. Policy and environmental implications of using HEFA+ for aviation. 2018. https://theicct.org/publications/policy-and-environmental-implications-using-hefa-aviation (accessed July 27, 2021).

(4) Nakhaei Pour, A.; Housaindokht, M. R.; Zarkesh, J.; Tayyari, S. F. Studies of carbonaceous species in alkali promoted iron catalysts during Fischer−Tropsch synthesis. *J. Ind. Eng. Chem.* **2010**, *16*, 1025−1032.

(5) Goel, P.; Boehman, A. L. Numerical simulation of jet fuel degradation in flow reactors. *Energy Fuels* **2000**, *14*, 953−962.

(6) Pelucchi, M.; Arunthanayothin, S.; Song, Y.; Herbinet, O.; Stagni, A.; Carstensen, H.-H.; Faravelli, T.; Battin-Leclerc, F. Pyrolysis and Combustion Chemistry of Pyrrole, a Reference Component for Bio-oil Surrogates: Jet-Stirred Reactor Experiments and Kinetic Modeling. *Energy Fuels* **2021**, *35*, 7265−7284.

(7) Zeng, P.; Wang, B.-Y.; He, R.; Liang, J.; Yang, Z.-Y.; Xia, Z.-X.; Wang, Q.-D. Single-Pulse Shock Tube Pyrolysis Study of RP-3 Jet Fuel and Kinetic Modeling. *ACS Omega* **2021**, *6*, 11039−11047.

(8) Wang, B.-Y.; Zeng, P.; He, R.; Li, F.; Yang, Z.-Y.; Xia, Z.-X.; Liang, J.; Wang, Q.-D. Single-Pulse Shock Tube Experimental and Kinetic Modeling Study on Pyrolysis of a Direct Coal Liquefaction-Derived Jet Fuel and Its Blends with the Traditional RP-3 Jet Fuel. *ACS Omega* **2021**, *6*, 18442−18450.

(9) Han, H. S.; Kim, C. J.; Cho, C. H.; Sohn, C. H.; Han, J. Ignition delay time and sooting propensity of a kerosene aviation jet fuel and its derivative blended with a bio-jet fuel. *Fuel* **2018**, *232*, 724−728.

(10) Dooley, S.; Won, S. H.; Chaos, M.; Heyne, J.; Ju, Y.; Dryer, F. L.; Kumar, K.; Sung, C.-J.; Wang, H.; Oehlschlaeger, M. A.; Santoro, R. J.; Litzinger, T. A. A jet fuel surrogate formulated by real fuel properties. *Combust. Flame* **2010**, *157*, 2333−2339.

(11) Dooley, S.; Won, S. H.; Heyne, J.; Farouk, T. I.; Ju, Y.; Dryer, F. L.; Kumar, K.; Hui, X.; Sung, C.-J.; Wang, H.; Oehlschlaeger, M. A.; Iyer, V.; Iyer, S.; Litzinger, T. A.; Santoro, R. J.; Malewicki, T.; Brezinsky, K. The experimental evaluation of a methodology for surrogate fuel formulation to emulate gas phase combustion kinetic phenomena. *Combust. Flame* **2012**, *159*, 1444−1466.

(12) Dooley, S.; Won, S. H.; Jahangirian, S.; Ju, Y.; Dryer, F. L.; Wang, H.; Oehlschlaeger, M. A. The combustion kinetics of a synthetic paraffinic jet aviation fuel and a fundamentally formulated, experimentally validated surrogate fuel. *Combust. Flame* **2012**, *159*, 3014−3020.

(13) Won, S. H.; Veloo, P. S.; Dooley, S.; Santner, J.; Haas, F. M.; Ju, Y.; Dryer, F. L. Predicting the global combustion behaviors of petroleum-derived and alternative jet fuels by simple fuel property measurements. *Fuel* **2016**, *168*, 34−46.

(14) *ASTM D6890-Standard test method for determination of ignition delay and derived cetane number (DCN) of diesel fuel oils by combustion in a constant volume chamber*; ASTM International, 2014.

(15) Calcote, H. F.; Manos, D. M. Effect of molecular structure on incipient soot formation. *Combust. Flame* **1983**, *49*, 289−304.

(16) Cho, C. H.; Han, K. R.; Sohn, C. H.; Haas, F. M. Sooting Propensity Estimation of Jet Aviation Fuel Surrogates and Their n-Alkane Components by the Virtual Smoke Point Method. *Energy Fuels* **2020**, *34*, 15072−15076.

(17) *ASTM D1322-Standard test method for smoke point of kerosine and aviation turbine fuel*; ASTM International, 2014.

(18) Mensch, A.; Santoro, R. J.; Litzinger, T. A.; Lee, S.-Y. Sooting characteristics of surrogates for jet fuels. *Combust. Flame* **2010**, *157*, 1097−1105.

(19) Westbrook, C. K.; Pitz, W. J.; Herbinet, O.; Curran, H. J.; Silke, E. J. A comprehensive detailed chemical kinetic reaction mechanism for combustion of n-alkane hydrocarbons from n-octane to n-hexadecane. *Combust. Flame* **2009**, *156*, 181−199.

(20) Malewicki, T.; Gudiyella, S.; Brezinsky, K. Experimental and modeling study on the oxidation of Jet A and the n-dodecane/iso-octane/n-propylbenzene/1, 3, 5-trimethylbenzene surrogate fuel. *Combust. Flame* **2013**, *160*, 17−30.

(21) Petersen, E. L.; Rickard, M. J. A.; Crofton, M. W.; Abbey, E. D.; Traum, M. J.; Kalitan, D. M. A facility for gas-and condensed-phase measurements behind shock waves. *Meas. Sci. Technol.* **2005**, *16*, 1716.

(22) Han, H. S.; Sohn, C. H.; Han, J.; Jeong, B. Measurement of combustion properties and ignition delay time of high performance alternative aviation fuels. *Fuel* **2021**, *303*, 121243.

(23) Burke, S. M.; Metcalfe, W.; Herbinet, O.; Battin-Leclerc, F.; Haas, F. M.; Santner, J.; Dryer, F. L.; Curran, H. J. An experimental and modeling study of propene oxidation. Part 1: Speciation measurements in jet-stirred and flow reactors. *Combust. Flame* **2014**, *161*, 2765−2784.

(24) Sen, F.; Kasper, T.; Bergmann, U.; Hegner, R.; Atakan, B. Partial oxidation of methane at elevated pressures and effects of propene and ethane as additive: experiment and simulation. *Z. Phys. Chem.* **2015**, *229*, 955−976.

(25) Song, Y.; Hashemi, H.; Christensen, J. M.; Zou, C.; Haynes, B. S.; Marshall, P.; Glarborg, P. An exploratory flow reactor study of H2S oxidation at 30−100 bar. *Int. J. Chem. Kinet.* **2017**, *49*, 37−52.
(26) Dooley, S.; Won, S. H.; Haas, F. M.; Santner, J. S.; Ju, Y.; Dryer, F. L.; Farouk, T. Development of reduced kinetic models for petroleum-derived and alternative jet fuels. *50th AIAA/ASME/SAE/ASEE Joint Propulsion Conference*; Cleveland, OH, 2014 AIAA 3661, July 28-30..
(27) Metcalfe, W. K.; Dooley, S.; Dryer, F. L. Comprehensive detailed chemical kinetic modeling study of toluene oxidation. *Energy Fuels* **2011**, *25*, 4915−4936.
(28) Mehl, M.; Curran, H.; Pitz, W.; Westbrook, C. K. *Chemical kinetic modeling of component mixtures relevant to gasoline*; Lawrence Livermore National Lab.(LLNL): Livermore, CA (United States), 2009.
(29) Gudiyella, S.; Brezinsky, K. High pressure study of 1, 3, 5-trimethylbenzene oxidation. *Combust. Flame* **2012**, *159*, 3264−3285.
(30) *CHEMKIN-PRO 2020 R1, Reaction Design*, San Diego, 2020.
(31) Haas, F. M.; Won, S. H.; Dryer, F. L. Detailed and compact combustion kinetic models for iso-dodecane and Gevo alcohol-to-jet (ATJ) alternative fuel. *2016 Spring Technical Meeting of the ESSCI*; Princeton University, 2016. March 13-16.
(32) Diévart, P.; Kim, H. H.; Won, S. H.; Ju, Y.; Dryer, F. L.; Dooley, S.; Wang, W.; Oehlschlaeger, M. A. The combustion properties of 1, 3, 5-trimethylbenzene and a kinetic model. *Fuel* **2013**, *109*, 125−136.
(33) Dussan, K.; Won, S. H.; Ure, A. D.; Dryer, F. L.; Dooley, S. Chemical functional group descriptor for ignition propensity of large hydrocarbon liquid fuels. *Proc. Combust. Inst.* **2019**, *37*, 5083−5093.
(34) Dahmen, M.; Marquardt, W. A novel group contribution method for the prediction of the derived cetane number of oxygenated hydrocarbons. *Energy Fuels* **2015**, *29*, 5781−5801.
(35) Won, S. H.; Haas, F. M.; Dooley, S.; Edwards, T.; Dryer, F. L. Reconstruction of chemical structure of real fuel by surrogate formulation based upon combustion property targets. *Combust. Flame* **2017**, *183*, 39−49.
(36) Abdul Jameel, A. G.; Naser, N.; Emwas, A.-H.; Dooley, S.; Sarathy, S. M. Predicting fuel ignition quality using 1H NMR spectroscopy and multiple linear regression. *Energy Fuels* **2016**, *30*, 9819−9835.
(37) Abdul Jameel, A. G.; Elbaz, A. M.; Emwas, A.-H.; Roberts, W. L.; Sarathy, S. M. Calculation of average molecular parameters, functional groups, and a surrogate molecule for heavy fuel oils using 1H and 13C nuclear magnetic resonance spectroscopy. *Energy Fuels* **2016**, *30*, 3894−3905.

https://doi.org/10.1021/acsomega.1c04002
ACS Omega 2021, 6, 26646−26658